Review of Scientific Instruments

Design of a high-throughput bio-ferrograph for isolation of cancer cells from whole blood

Cite as: Rev. Sci. Instrum. **92**, 074103 (2021); https://doi.org/10.1063/5.0053038
Submitted: 03 April 2021 . Accepted: 23 June 2021 . Published Online: 07 July 2021

D. Svetlizky, O. Levi, and N. Eliaz

AIP Publishing

Review of Scientific Instruments ARTICLE scitation.org/journal/rsi

Design of a high-throughput bio-ferrograph for isolation of cancer cells from whole blood

Cite as: Rev. Sci. Instrum. 92, 074103 (2021); doi: 10.1063/5.0053038
Submitted: 3 April 2021 • Accepted: 23 June 2021 •
Published Online: 7 July 2021

D. Svetlizky, O. Levi, and N. Eliaz[a)]

AFFILIATIONS

Biomaterials and Corrosion Laboratory, Department of Materials Science and Engineering, Tel Aviv University, Ramat Aviv, Tel Aviv 6997801, Israel

[a)]Author to whom correspondence should be addressed: neliaz@tau.ac.il

ABSTRACT

Enumeration and morphological characterization of circulating tumor cells (CTCs) can be useful in diagnosis and prognosis of metastatic cancer patients. The bio-ferrograph (BF) with its five flow channels, which was developed in the late 1990s for magnetic isolation of biological cells and tissue fragments from fluids, is a modification of the analytical ferrograph. Its use for isolation of rare CTCs from human whole blood (HWB) is a novel approach for the detection of cancer at a cellular level. The isolation process is facilitated by the interaction of specifically magnetized cells with a strong external magnetic field, yielding high recovery rates with no morphological alternation of cells that are isolated on a coverslip glass slide, thus allowing complementary microscopic, chemical, biological, and mechanical analyses. Here, a full mechanical and magnetostatic design of a novel high-throughput BF is presented. The system design is based on an optimized procedure for bio-ferrographic isolation of CTCs from HWB. It incorporates a semi-automated CTC separation system consisting of sample preparation, labeling, and staining; magnetic isolation; and system recovery. The design process was optimized based on experimental feasibility tests and finite element analyses. The novel bench-top system consists of 100 flow channels, allowing simultaneous analysis of multiple samples from 20 patients in each run, with the potential to become a decision-making tool for medical doctors when monitoring patients in a hospital setting. It opens a new route for early diagnosis, prognosis, and treatment of cancers, as well as other diseases, such as osteoarthritis.

I. INTRODUCTION

Ferrography is a magnetic health/condition monitoring technique that allows the separation of ferromagnetic and paramagnetic particles from a liquid onto a glass slide under a strong external magnetic field.[1–3] Based on the number, size, shape, surface morphology, and chemical composition of the isolated magnetic particles, the level, origin, and mechanism of wear can be determined.[1] Since its invention in the early 1970s, ferrography has been found reliable and sensitive for monitoring wear evolution in engineering systems such as helicopter gearboxes.[1] These are typically closed-loop systems, although the applicability of ferrography to an open-loop oil system was demonstrated too.[4]

Approximately 25 years after the invention of the analytical ferrograph, the bio-ferrograph (BF) was invented to capture target biological matter such as cells and tissue fragments from body fluids.[5,6] The magnetization of the biological matter can be either non-specific (using solvents that contain rare earth salts, most commonly $ErCl_3$) or specific (using antibodies conjugated to magnetic beads).[1,2] In order to increase the sensitivity and to be able to isolate smaller particles with a weaker magnetic moment, the strength of the magnet was increased, the fluid flow direction was changed from near-horizontal to vertical, and the thickness of the microscope glass slide on which the isolated particles are deposited was reduced.[1,2] The trade-off in this deposition scheme, however, is that larger/denser particles are no longer deposited preferentially upstream of smaller/less dense particles.[1] The BF allows flowing simultaneously up to five fluid samples through five distinguishable bracketed areas on the coverslip slide, without cross-contamination.[1,2] Other advantages of BF compared to filtration or other immunomagnetic isolation (IMI) techniques include quantitative analysis of the captured biological matter while observing it microscopically, extremely high selectivity and sensitivity, very high recovery rates, small and confined deposition area, preservation of the structure and morphology of the isolated particles, the ability to analyze different isolated cells simultaneously, applicability to any liquid sample (including whole blood), and the ability to capture particles as small as several nanometers.[1,2,7,8]

Bio-Ferrograph 2100, from Guilfoyle, Inc.,[1,2,6] is a bench-top, cytometry-based, high-gradient magnetic field separator. The magnetic field is generated by an interpolar gap of a ferrite-based (SrFe) permanent magnet assembly and a pair of low-carbon steel pole pieces. The interpolar gap forms a magnetic barrier to both inherently magnetic and magnetized particles suspended in a liquid. The maximum magnetic flux density formed across the interpolar gap was reported to be between 1.67[9] and 1.8 T.[1] The gradient of the field is maximal at the edges of the interpolar gap, where most particle deposition takes place, thus forming two parallel particle strips—primary and secondary—on the ferrogram (the microscope coverslip slide with deposited particles).[1,2,7] Consequently, a rectangular deposition band can be observed on the ferrogram, often even by naked eye. The Bio-Ferrograph 2100 system utilizes a simple five-syringe pump assembly that allows the simultaneous processing of five samples under identical flow and magnetic field conditions. Such a design allows running control samples together with the actual samples. One of the main advantages of such a magnetic separator is the freedom that it provides to utilize a wide variety of complementary sample manipulation and characterization of the isolated particles, thanks to the optical transparency, mechanical rigidity, smooth surface, and low chemical reactivity of the coverslip slide.

To date, bio-ferrography and related technologies of magnetic flow sorting [such as magnetic deposition microscopy (MDM), and bactography] have been used successfully to track bacteria[10–24] and malaria,[25–27] capture rare magnetic minerals embedded in a *Vespinae* comb,[28] separate between carbon micro- and nanoparticles suspended in ethanol,[8] isolate bone and cartilage tissue fragments from the synovial fluids in human joints for diagnosis of osteoarthritis (OA),[2,29] determine the efficacy of a pain-relief drug treatment,[2,30] and isolate both polymeric and metallic wear particles from artificial joints for mechanical wear evaluation.[1,2,31–33] For the purpose of OA evaluation, for example, magnetization of the target tissue fragments was achieved by mixing the synovial fluids with cocktails containing monoclonal anti-collagen I and anti-collagen II antibodies coupled to 50 nm paramagnetic magnetic-activated cell sorting (MACS^{TM}) MicroBeads.[29,30]

Bio-ferrography and MDM have also been used to isolate and characterize mechanically cancer cells, with some exciting results.[7,34–39] Circulating tumor cells (CTCs) detach from primary or metastatic lesions and circulate in the peripheral blood. Liquid biopsy, enumeration of CTC, and their single-cell morphological (microscopic) and molecular/genetic analyses could provide significant clinical information for cancer diagnosis, assessment of recurrent risk, prognosis, and therapeutic strategies.[40–47] CTCs also have some important advantages compared to circulating tumor DNA (ctDNA) and contribute complementary information.[47] Unfortunately, CTCs have low prevalence in the blood circulation [one to ten CTCs compared to a few million white blood cells and a billion red blood cells in 1 ml human whole blood (HWB)],[41,43] their half-life in blood is short (~1 to 2.4 h),[42] and only a limited number of them have metastatic capacity.[42] Therefore, exceptionally high sensitivity, high specificity, low value of limit-of-quantification (LOQ), and high recovery rates are expected from any technology for isolation of CTCs from liquid biopsy.

Epidermal growth factor receptor (EGFR)-overexpressing tumors include colorectal cancer (CRC), the third most commonly diagnosed cancer and the second leading cause of cancer death, which suffers from a lack of diagnostic techniques that are both effective and noninvasive.[7] In Ref. 7, bio-ferrography was used to separate between target (positive) A431 cells, which simulate EGFR-overexpressing epithelial CTCs, from NIH 3T3 mouse embryo fibroblast nontarget (background or negative) cells. Sample analysis was also made by MACS (Miltenyi Biotec, Bergisch-Gladbach, Germany) and EasySep^{TM} (Stemcell Technologies, Vancouver, BC, Canada). Bio-ferrography was claimed to apparently have some significant advantages also compared to the semiautomated CellSearch^{TM} (Menarini Silicone Biosystems, Florence, Italy), the only validated method for CTC monitoring that has been cleared by the US FDA.[7,48–50] The main disadvantages of CellSearch are that CTCs lacking EpCAM expression cannot be captured and that this closed system does not allow easy access to the captured CTCs for complementary molecular, morphological, and other characterization.[48,49]

Levi *et al.*[36] employed a design of experiment (DOE) methodology to both minimize the number of experiments necessary given 21 variables in the procedure (2^{21} = 2 097 152 experiments!) and optimize the bio-ferrographic CTC isolation procedure. An exceptional recovery rate of up to 97% was achieved when 2–100 CTCs were suspended in 1 ml HWB. The optimized bio-ferrographic isolation process was later validated in a preliminary clinical study on CRC patients (unpublished data). For comparison, CellSearch was reported capable of capturing at least two CTCs per 7.5 ml blood sample in only 99 out of 333 (~30%) of metastatic CRC patients.[51] Furthermore, CellSearch^{TM} revealed maximum 50 captured cells in CRC patients. Normalizing this number by the blood sample volume (7.5 ml), one can expect to typically observe maximum six to seven cells on a ferrogram prepared from 1 ml blood sample, which matches the observations of Levi *et al.* The aforementioned results highlight the attributes and strengths of bio-ferrography for the isolation of CTCs from HWB and position it as one of the most promising technologies for detection and analysis of CTCs.

Here, a full mechanical and magnetostatic design of a novel, high-throughput, sensitive BF-based medical device for the separation of CTCs from HWB is presented. The novel bench-top bio-ferrographic system[52] contains 100 flow channels (compared to five in Bio-Ferrograph 2100) that allow analyzing 20 patients simultaneously. The new system is also more automated in the run process, but also heavier, than Bio-Ferrograph 2100. It will allow analysis of up to 20 patients at a time, a requirement set to make it useful in hospitals. The system design is based on the current optimized procedure for bio-ferrographic isolation of CTCs from HWB. It incorporates a semi-automated CTC separation system consisting of sample preparation, labeling, and staining; magnetic isolation; and system recovery. The design process was optimized based on experimental feasibility tests and finite element analysis (FEA). The complete design included reverse engineering of a BF magnetic core, magnetostatic and structural FEA simulations, flow system design, design of custom mechanical components, enclosure design, full 3D computer-aided design (CAD) of the system, material and component selection, and feasibility experiments. The new instrument has the potential to become a decision-making tool for medical doctors when monitoring patients in a hospital setting. It opens a new route for early diagnosis, prognosis, and treatment of cancers. Moreover, it can be adjusted for other biomedical applications, for example,

diagnosis, prognosis, and treatment of OA. Its market and beneficiaries include patients, medical doctors, medical organizations, and companies that develop biomarkers, drugs, medical diagnostics, and disease treatments.

II. DESIGN OF A NOVEL MULTI-CHANNEL BIO-FERROGRAPH

In this study, we implemented a prescriptive design model for the design of technical systems and products.[53] The system design block diagram is presented in Fig. 1 and is composed of two main subsystems: (1) controlled flow subsystem (for reagent delivery, priming, and system recovery) and (2) isolation subsystem. Other subsystems, namely, electricity, control, refrigeration, and enclosure,[52] are not discussed herein.

The designed system[52] is sustained with the following external inputs: (1) 100 tubes filled with 1 ml blood samples, (2) biological and recovery reagents, and (3) 20-slide rack. The system's output consists of 20 slides, which are associated with 20 patients, where each slide has five channels of isolated CTCs according to the optimized bio-ferrography protocol.[36] The optimized bio-ferrography-based CTC isolation procedure utilizes several operations with different pieces of equipment:[36] centrifuge, orbital shaker, cooling devices, and optical and fluorescence microscope. Specific changes in the isolation protocol can be excluded if they do not result in an apparent change in recovery rate. Hence, procedures that involve centrifuge were excluded from the system requirements and were replaced by primary washing of the patient blood sample. The step of washing excess antibodies and microbeads, which follows the cocktail-blood incubation, was excluded too. In contrast to the single-use BF flow system (disposable cassette, priming cups, and syringes), the designed system is reusable. It utilizes high-precision metering pumps, reusable tubes, and manifolds (tube rack, needles, and coverslip slides are disposable). Therefore, a system recovery procedure was developed.

In summary, the designed system consists of the following steps: (1) blood sample preparation and IM labeling, (2) isolation procedure, and (3) system recovery.[52] The system design process accounts for possible requirements of the operator, medical decision-maker, and maintenance team.

III. CONTROLLED FLOW SUBSYSTEM

The flow system is responsible for the delivery of reagents in an accurate and controlled manner. Each stage in the system operation requires its own reagents, as listed in Table I. To meet both the biological procedure and technical requirements, a conceptual design of the flow system was made, as illustrated by the flow diagram in Fig. 2. This design includes the definition of the flow direction in any pipeline, the intersections, and the locations of the pumps, reservoirs, valves, manifold, and tubes.

The design of the flow system was divided into two main phases: (1) accurate portion delivery of the ingredients from the required reservoir tubes into a control volume manifold and (2) transportation of the ingredients from the control volume manifold into the target tubes. According to this system's flow pattern, the ingredients are prepared and installed by the operator at the designated location in the refrigeration system. Each ingredient is

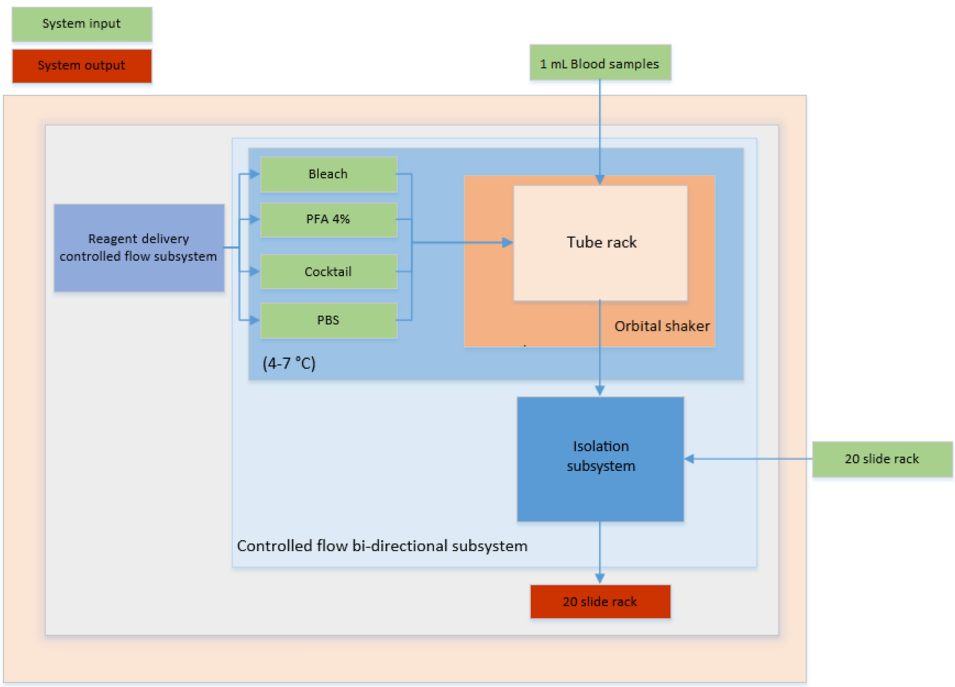

FIG. 1. System block diagram. Phosphate-buffered saline (PBS) is used in all stages of IM labeling, fixation, priming, and recovery. Cocktail is used for IM labeling, 4% paraformaldehyde (PFA) is used for fixation, and bleach is used for recovery.

TABLE I. Required reagents in each stage of the procedure.

Procedure stage	Reagents
Blood IM labeling	Antibody cocktail, PBS
Fixation	4% PFA, PBS
Priming	PBS
Recovery	Bleach, ethanol, PBS

pumped by its corresponding pump (A–D) through a designated disposable needle and Tygon tube to the entry of the control volume manifold (priming). This step facilitates the ability to deliver a precise amount of fluid at each stage of the delivery of the ingredients using a metering pump with a precisely controlled volume [low-flow miniature original equipment manufacturer (OEM) pump with a dispense rate of 0–25 μl/revenue]. The control volume manifold is equipped with one-way check valves in order to ensure that the inlet

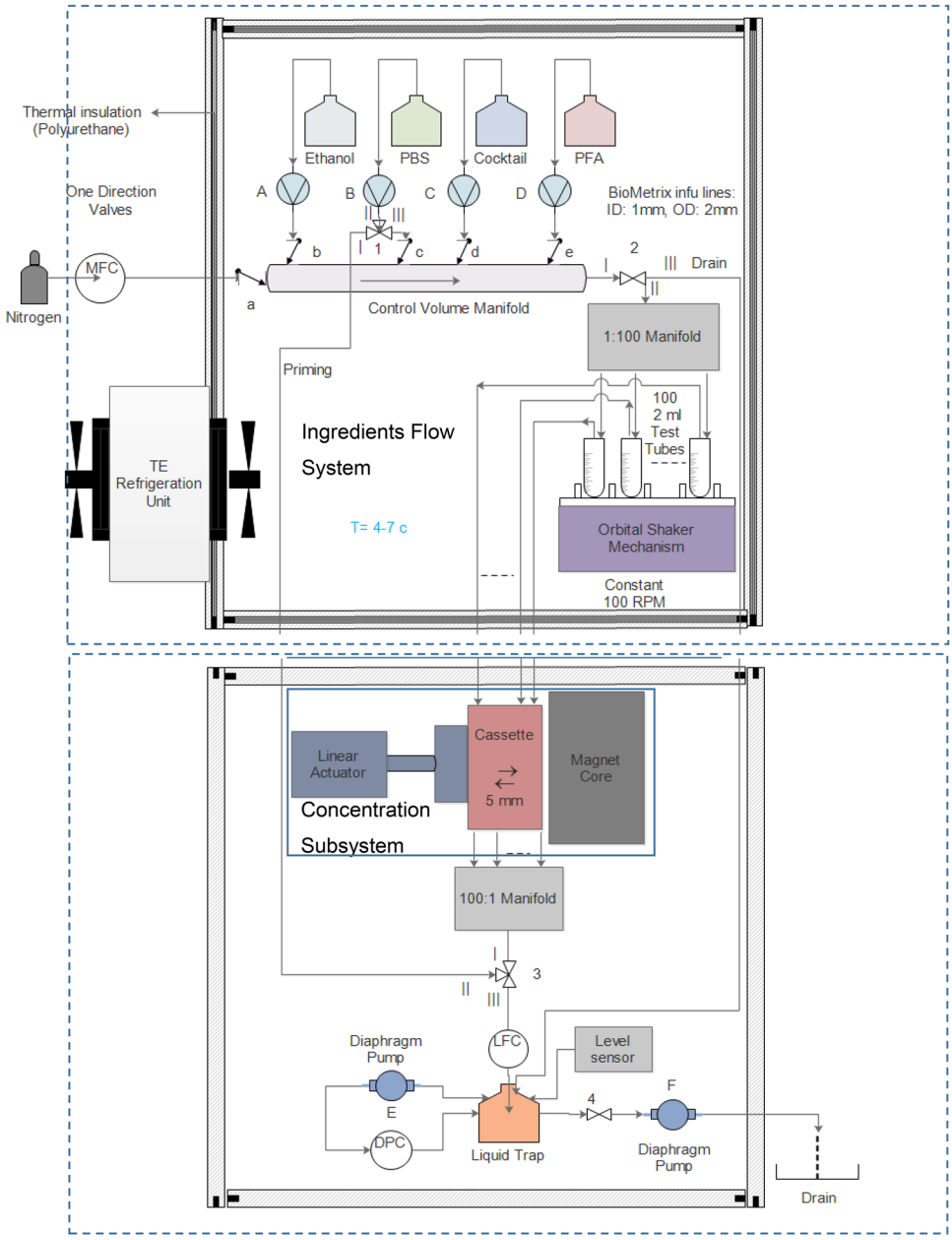

FIG. 2. Flow system piping and instrumentation flow diagram.

lines remain primed and that the pump dispense accuracy will not decrease due to pressure changes in the control volume manifold. Following the priming stage, the delivery flow system is ready for use. According to each process, the appropriate pump delivers the precise required volume of fluid into the control volume manifold. The fluid is then delivered by a nitrogen gas pressure flow, which "pushes" it through the Tygon tubes in the circular manifold into the corresponding test tubes. The gas flow rate is controlled by a mass flow controller that enables a stable flow rate with responsive control of the process flow rates and pressures and real-time readings. This delivery concept enables the delivery of the reagents with minimal residues in the tubes and minimal waste. In order to reduce the inlet pressure of the mass flow-up controller to a workable level (maximum 1 bar), a two-stage gas pressure regulator was integrated into the flow system. It provides a constant delivery pressure, with no need for periodic readjustment.

The reusable tubes that are integrated into the reagent delivery subsystem design are made of medical grade PVC (DEHP-free) with an inner diameter (ID) of 1 mm and an outer diameter (OD) of 2.1 mm. This tube material was selected due to its high resistance against the chemicals in use. An essential subsystem requirement is that the flow system facilitates full system recovery for subsequent system use. However, the cleaning of the outer tube surface area that is in contact with blood is highly challenging, time demanding, and expansive. Hence, the use of disposable needles and tubes was chosen. In this subsystem, contamination of the outer surface of both the tubes that pump the reagents (Fig. 2) and the tube array outlet (Fig. 3) might occur. The needles are designed to be easily mounted and replaced in the tube mounting plate.

In the case of contamination of the tubes that are mounted on the blood tube rack, a more complex design solution was needed. The blood tube rack is assembled of 100 tubes, but manual disassembly of 100 needles is not practical. The solution concept involves a design of 10 × 10 disposable tube array, which is easy and efficient. This disposable tube array is immersed in the blood tubes on one side [Fig. 3(a)], and on the other side is connected to a negative array of tube connectors, which is connected to the outlet tube lines of the 1:100 manifold [Fig. 3(a)]. This connection fitting between the arrays facilitates proper flow in two directions: The first is the delivery of reagents into the blood tubes, while the second is the delivery of the blood samples from the tube through the isolation system in the CTC isolation process (Fig. 2). In total, each of the connection fitting arrays is assembled of 200 tube fittings—100 tubes for the reagents delivery into the blood samples and another

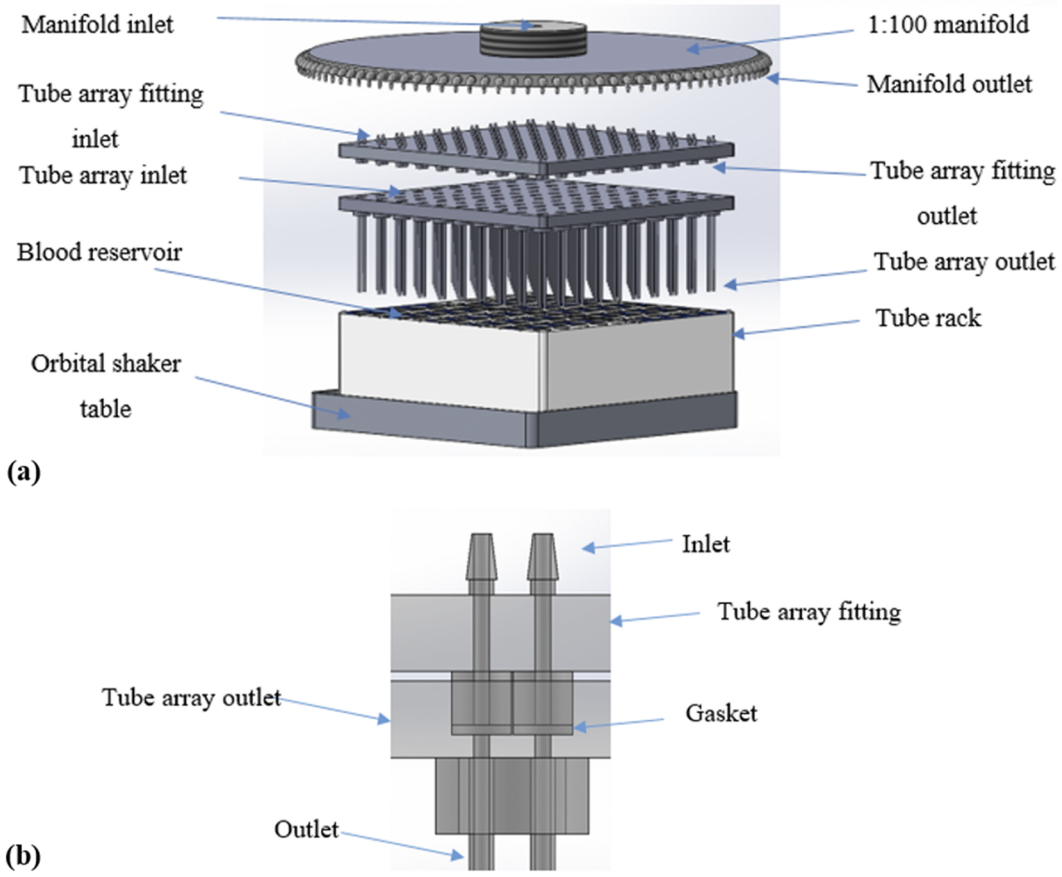

FIG. 3. (a) Flow-line connection in exploded view. (b) Cross sectional assembly view of the tube array sealing.

100 tubes that deliver the blood through the isolation system (Fig. 3).

At the end of the outlets, a flat, 1-mm thick ethylene propylene diene monomer (EPDM) rubber gasket (50 Shore A hardness) is glued. Following the connection of the two, the gasket is squeezed between the mating surfaces as they are clamped together [Fig. 3(b)]. This facilitates proper flow of the reagents to the blood test tubes and from there—toward the isolation system, with no dead volume for blood clotting. The loading force that is required to achieve proper sealing of the gasket and to prevent leakage of the tube fitting was experimentally determined via a compression test. The tested gasket was made of EPDM, 50 Shore A hardness, width 1 mm, ID 1 mm, and OD 3.9 mm. Compression test results showed that a load of 6.2 N was needed for 20% deflection of the gasket seal. In total, the tube array fitting is assembled with 200 gasket seals; thus, a compressive force of 1240 N in total is required to facilitate a proper seal between the tube array fitting and the tube array. This is established by an operator's manual tightening of designated four socket head cap screws, which are located at each corner of the tube array fitting.

Following a pre-isolation stage, which involves IM labeling and incubation, a priming stage is required. The isolation flow lines are filled with PBS to prevent air bubbles from forming in the flow lines and flow channels. The formation of air bubbles might significantly reduce the recovery rate due to the change in the flow regime and possible blood encapsulation in the formed air bubbles. Since the designed ingredients' flow subsystem is integrated with a PBS reservoir and an assigned metering pump, the concentration system flow lines priming can be easily performed without adding an additional PBS reservoir. Using a three-way controlled valve system (valve 1, path I-II; valve 3, path I-II), made of Series 1 three-way diaphragm polytetrafluoroethylene (PTFE) valve, through which the PBS is pumped, and a 1:100 manifold, the PBS shall flood the cassette flow channels and fill the blood sample tubes to a final volume of 2 ml. Following the priming stage and using the assigned PBS pump, pipetting and mixing of the PBS-blood samples are executed to improve the sample homogeneity.

Following the pre-isolation stage, which consists of blood IM labeling, incubation, and priming, the system is ready for the CTC isolation stage. Since one of the flow system requirements is to facilitate continuous flow through the flow lines, a diaphragm pump operated in the vacuum mode was utilized. It allows continuous flow in the system's flow lines when integrated with a liquid trap design, which acts as a pulse flow dumper, at the specified flow rate. In addition, the liquid trap allows meeting the requirement for non-contamination of the flow matter since the flowing matter does not flow through the pump (Fig. 2).

The flow pattern in the isolation stage is as follows. The diaphragm pump (pump E) draws existing air in the liquid trap to a specific, constant, negative pressure value. The pump cannot lock pressure; therefore, a gas dual pressure controller (DPC, PCD series, −15 to 0 psi) was integrated to maintain a constant and stable pressure during the whole isolation stage. The defined pressure value in the liquid trap is the main parameter that determines the accepted flow rate through the isolation flow system's lines. The liquid trap outlet is connected to a liquid flow controller (LFC), which controls the concentration flow rate at a precise and constant value. When the three-way controlled valve (valve 3, paths I–III, Fig. 2) is opened, the 100 blood samples are drawn from the tube rack through the tube array fitting and the magnetic core flow channels at a constant flow rate of 0.021 ml/min. As the blood samples pass through the magnetic core, the samples flow through the controlled valve and are gathered to a single flow line via a 100:1 manifold and are poured into the liquid trap. The LFC stops the isolation process after pumping 1.9 ml of the sample (which takes ~90 min) to avoid the entrance of air into the flow lines.

The fixation stage consists of delivery of 4% PFA into the flow channels, 20 min incubation, and washing of the whole flow system with PBS. This is done using the reagent delivery flow subsystem and the isolation flow subsystem, as described above. The LFC stops the isolation process once the PFA fills the flow channels (the sample tubes are filled with PFA up to the tube array fitting tubes' inlet) in order to avoid the entrance of air into the flow lines.

Once the isolation process is completed, the system is ready for the recovery stage. The slides are disassembled and replaced with a new recovery set slide case assembled with 20 new slides. In order to prepare the flow system for the recovery stage, the manifold and the connected flow lines are first washed with ethanol, using pump A and the nitrogen flow system through valve 2 (paths I and II). Next, reservoirs B–D are disassembled, followed by drainage of pumps B–D of ramming residues in the connecting flow lines into the control volume manifold. Using the nitrogen delivery system and valve 2 (paths I–III), the remaining residues are delivered to the liquid trap. At this stage, the disassembled reservoir needles are replaced with new ones by installing three reservoirs (B–D) filled with bleach. The sample tube rack and the disposable tube array fitting are replaced with new ones to prevent flow line contamination during the recovery stage.

The recovery stage itself comprises two washing steps: bleach and ethanol. It starts by washing the flow lines with bleach, by drawing bleach to the tube rack (pumps B–D, valve 2, paths I–II), and by nitrogen flow, followed by drawing of the bleach through the magnetic core using pump E and valve 3 (paths I–III) to the liquid trap. The system priming flow lines are washed as well, using pump B, through valve 1 (paths I and II) and valve 3 (paths II–III) into the liquid trap. Before proceeding to the second stage, reservoirs B–D are replaced with three reservoirs filled with ethanol. Pumps A–D draw ethanol to the tube rack and the magnetic core, as described in stage 1. In addition, using pump B and valve 3 (paths II–III), ethanol is drawn through the priming flow lines to the liquid trap.

When both the isolation and recovery stages are completed, the waste is disposed from the liquid trap through valve 4 (two-way diaphragm PTFE valve) and a drainage pump F to an external drainage. In order to ensure that the blood sample waste is not drawn into the diaphragm pump, a magnetic liquid level switch was integrated into the system design.

IV. MAGNETIC ISOLATION SUBSYSTEM

The magnetic isolation system of Bio-Ferrograph 2100 forms a high-gradient magnetic field, which is generated by a single interpolar gap of a permanent magnet core. The unique assembly of the SrFe permanent magnets, the magnetic isolator prism (pole shim) made of Aluminum 1060 alloy, and the magnetic pole piece conductors made of AISI 1010 low-carbon steel create a closed circuit of the magnetic flux (Fig. 4). The width of the interpolar gap defines

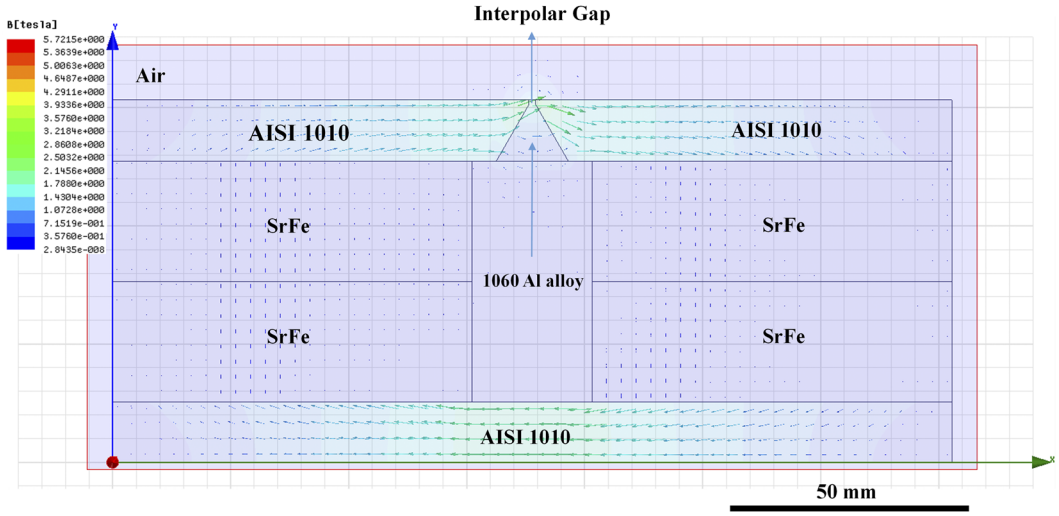

FIG. 4. Magnetic field vector flow, demonstrating a closed circuit of the magnetic flux based on a single interpolar gap.

the intensity of the magnetic flux at the gap edges. With a proper width, a high magnetic flux gradient is formed, which enables the maximal magnetic field at both edges (in opposite directions) of the interpolar gap. The absolute values of the magnetic field flux are maximal at the edges of the interpolar gap at the upper surface of the assembly and decrease sharply as the distance from the interpolar gap surface increases. As part of the system design requirements, the CTC isolation system is able to analyze up to 100 flow channels simultaneously. Hence, a modification of the magnetic core was performed.

Two modified configurations were examined, Fig. 5(a)–extended configuration and parallel configuration. The extended configuration is based on extension of the interpolar gap length. In this approach, there is no actual difference in the magnetic field value at the interpolar gap in comparison to the magnetic core assembly of Bio-Ferrograph 2100 due to the plane symmetry of the magnetic core. The main drawback of this configuration is the resulting large physical dimensions of the magnetic core assembly. The parallel configuration approach is based on a parallel assembly of several interpolar gaps parallel to each other. A four-capture-band parallel configuration was designed to enable simultaneous analysis of 20 slides with the most compact dimensional configuration, Fig. 5(b).

FEA magnetostatic analysis (Maxwell 16.0, ANSYS, Inc., Canonsburg, PA, USA) was utilized to validate that the formed magnetic field magnitude established at the four-interpolar-gap magnetic core is consistent and satisfying. The simulation was defined to solve Maxwell's equations (by a Gaussian elimination method) for the static magnetic field of a given permanent magnetic core geometry, materials, and boundary conditions [see Fig. 6(a)] over a finite region of space.[54,55] The 3D problem was reduced to a 2D problem, considering the problem's plane symmetry as the magnetic field is identical at each section of the element normal to the z-axis, neglecting end effects. The analysis was done in gradual steps by changing the number of the six-node quadratic triangle element, until the convergence value of the magnetic field target parameter was achieved. The graduate mesh refinement was used by an automatic adaptive meshing. Both the number of elements and the number of passes are determined by the initial convergence target of the energy error percent (which was set to 10^{-5}). Following the mesh refinement iteration process, 31 passes of solution were acquired for convergence of the magnetic field magnitude. At the convergence pass, the total number of mesh elements was $\approx 1.07 \times 10^6$, with a mean element area of 6.34×10^{-8} mm^2. The FEA magnetostatic model was first validated by comparing the simulated results of the traditional BF 2100 single-gap magnetic core to a reference measurement by a Gaussmeter measuring device.[56]

Figure 6 demonstrates the magnetic field gradient around the interaction interface of the pole piece, the insulator material, and the air region. Though the maximal value of the magnetic field magnitude at the edges of the interpolar gap is allegedly 5.464 T, this is not the apparent magnetic field that the CTCs passing through the flow channel sense. One should consider that the maximal magnetic field magnitude is located at the sharp corner of the gaps, where a singularity of the magnetic field solution occurs.

The FEA results match well the measured magnetic field. The magnetostatic simulation results show that the four-capture-band parallel configuration magnetic core creates a closed circuit of the magnetic flux, enabling the appearance of a maximal magnetic field gradient at the interpolar gap [Fig. 6(a)]. As shown in Figs. 6(a)–6(c), the magnetic field is maximal at the edges of the interpolar gap at the magnetic core's upper surface and decreases sharply as the distance increases from the interpolar gap surface. These results match well the field distribution for the one-isolation band magnetic core configuration in the Bio-Ferrograph 2100 system. Figure 7 shows the change of the magnetic field along the lateral axis at 0.15 mm from the magnet's top plane.

The FEA magnetostatic analysis reported herein is somewhat different from previous work by Nath *et al.*[57] who utilized a multi-stage parallel configuration permanent type magnet for increasing

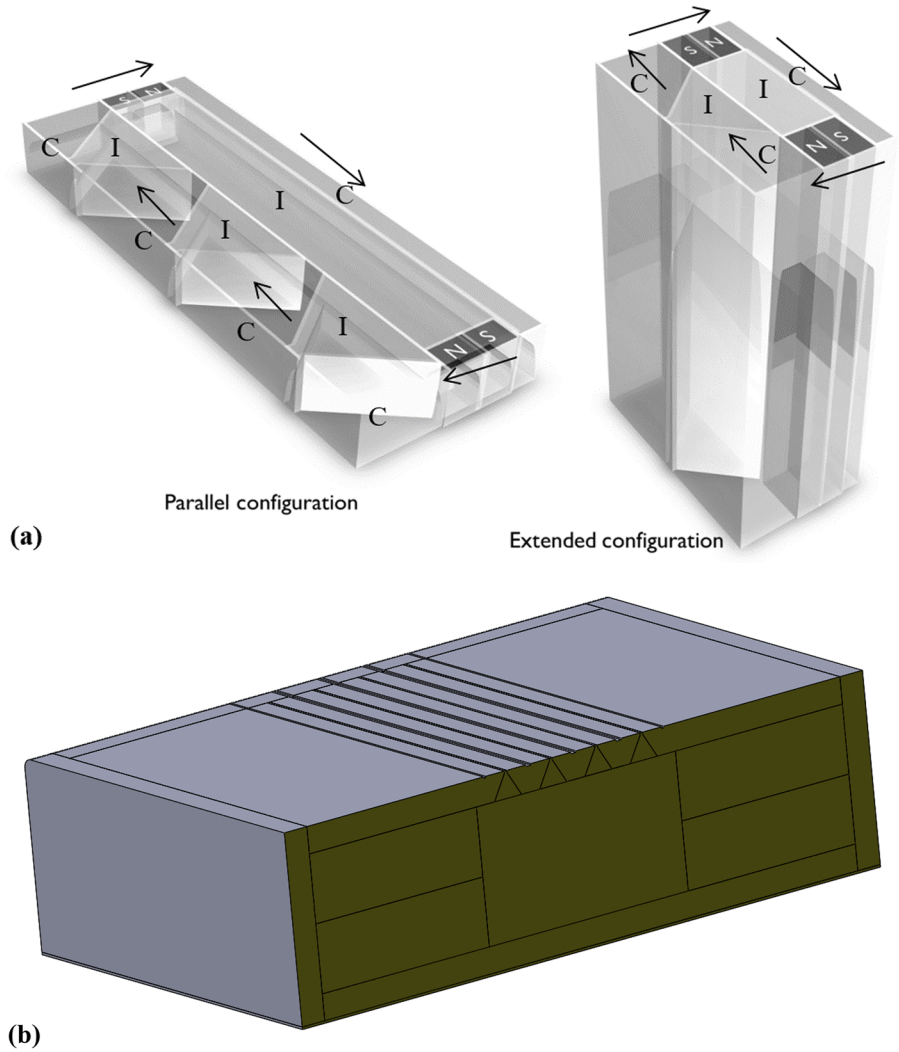

FIG. 5. (a) Parallel and extended configurations of the magnetic core. Magnetic flux direction (arrows), isolation material components (I), and conduction material components (C) are labeled. (b) A parallel configuration of the magnetic core with a four-capture-band assembly, 3D isometric with a cross sectional view (green plane).

the cell capturing efficiency of magnetically and fluorescently labeled Jurkat cells. It is also different from previous work by Sun *et al.*[58] where FEA was used to map the magnetic field in combination with laminar flow conditions to theoretically predict the trajectory of intrinsically magnetic spores and red blood cells in a flow channel of a MDM system.

The actual magnetic field magnitude that the CTCs sense while passing through the flow channel should be considered across the actual thickness of the glass coverslip. The influence of coverslip thickness on the simulated magnetic field with a significant distance of the singularity points was analyzed (Table II). The manufacturer's tolerance of coverslip glass slide No. 0 (0.08–0.15 mm) is considered. As expected, due to the high magnetic field gradient at the interpolar gap edge, a significant decrease in the magnetic field occurs with the increase in the slide thickness. An interesting phenomenon arises, resulting from the parallel magnetic core configuration—a "bath" type distribution of the maximal magnetic field magnitude at the interpolar gap edges (corresponding to the results presented in Table II). This type of behavior could be expected due to both the plane symmetry of the problem relative to the *y*-axis and the change in the distance of the interior gaps (i.e., gaps 2 and 3) and the external gaps (i.e., gaps 1 and 4) relative to the magnetic cores that are placed on both sides of the magnetic core assembly. Despite this phenomenon, the difference in the simulated magnetic field between the interior interpolar gap edges 2 and 3 and the exterior gap edges 1 and 4 is relatively negligible (~0.07 T). Thus, the suggested design is expected to be suitable for the magnetization of CTCs.

The obtained FEA magnetostatic analysis results of the parallel configuration magnetic core were also compared with the single interpolar gap magnetic core configuration. Zborowski *et al.*[9] reported a calculated magnetic field of 1.67 T at the interpolar edges at an average coverslip No. 0 thickness of 0.11 mm. The field value was extrapolated from the field measurements taken as a function of distance from the interpolar gap. This report is consistent with the FEA of the four-band parallel magnetic core configuration (Table II). The above discussion shows that the suggested magnetic core with a parallel configuration is applicable for the isolation of CTCs.

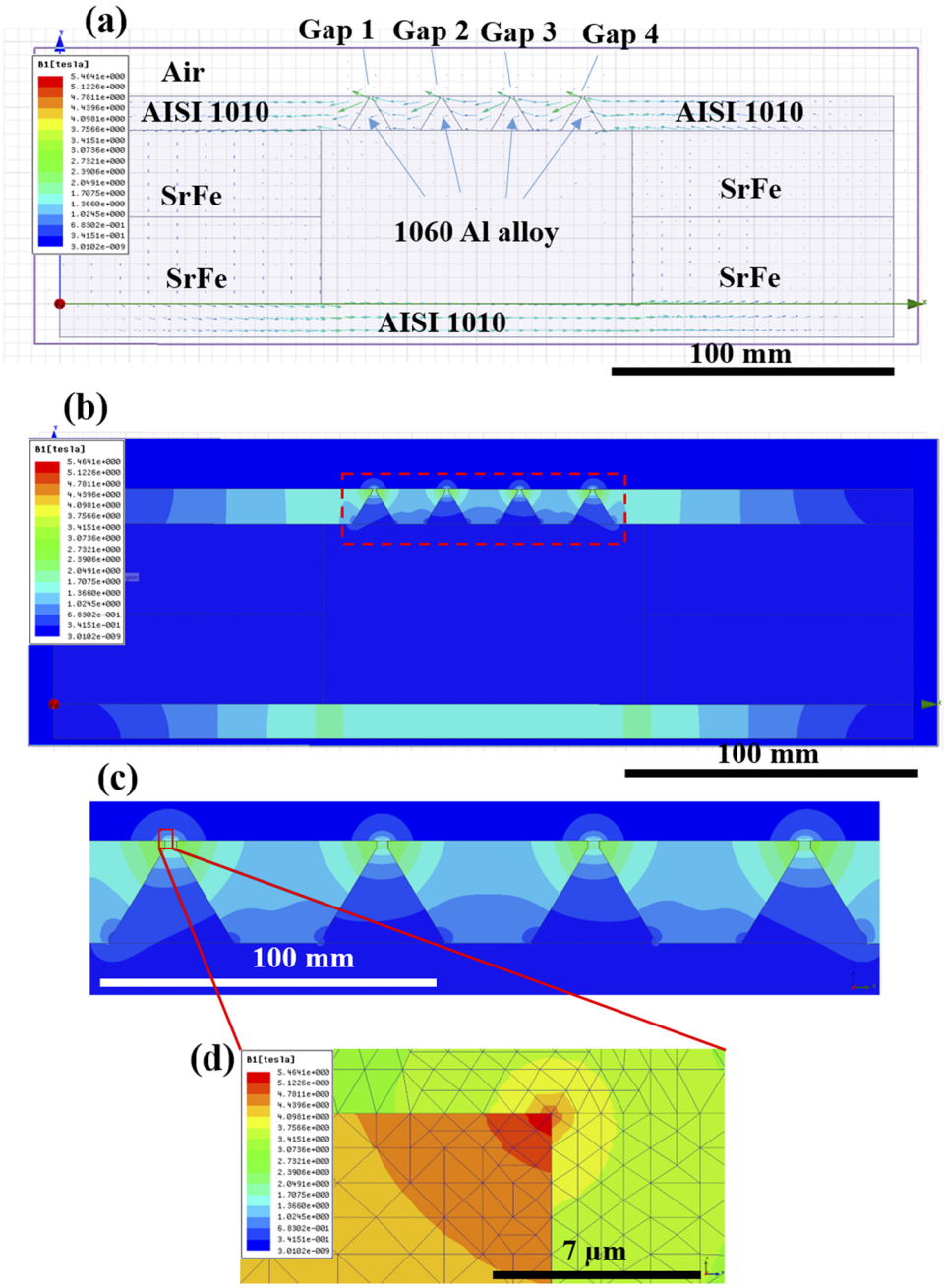

FIG. 6. (a) Magnetic field vector flow, demonstrating a closed circuit of the magnetic flux. (b) Magnetic field magnitude of the magnetic core assembly. (c) Magnification of the magnetic field magnitude at the labeled area in (b). (d) Magnification of the magnetic field magnitude at the labeled area in (c), demonstrating the high magnetic field gradient very close to the interpolar gap.

V. CASSETTE-MAGNET SEALING SUBSYSTEM

The new system is designed to have a reusable cassette system that facilitates 100 flow channels. The cassette-magnet subsystem design was divided into two parts: (1) cassette and slide assembly and (2) cassette-magnet tightening.

The conventional Bio-Ferrograph 2100 uses a disposable cassette, which is attached to a designated silicone gasket and a single coverslip slide. This type of assembly forms five individual flow channels after installation onto the magnetic core. The cassette installation is facilitated using two latches, which generate a force of ~250 N on each side of the cassette in order to prevent leakage.

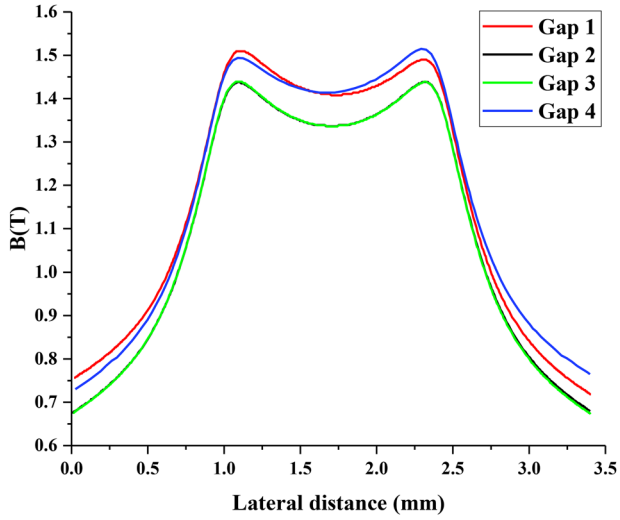

FIG. 7. Change in the simulated magnetic field of the four interpolar gaps along the lateral axis on the magnetic core surface.

In order to facilitate 100 reusable flow channels, a new concept of cassette and slide assembly was designed. The cassette-slide assembly design allows the operator to install 20 slides into the system at once, using the coverslip slide rack [Fig. 8(a)] while establishing 100 flow channels quickly and conveniently in a precise location over the magnetic core. The installation of the slides is done by the operator by inserting the slides into a designated slot on the magnet surface. The flow channels are formed by tightening permanent O-ring seals, which are installed in curved grooves at the backside of the cassette, toward the coverslip slide [Fig. 8(b)]. Tygon tubes are permanently connected to the cassette's backside, so the samples are able to enter the flow channels and exit through the outlet Tygon tubes to the drain [Figs. 8(c) and 8(d)]. The permanent O-ring seal is a key component in the tightening system, which allows the establishment of the flow channels between the coverslip slide and the magnetic core. As shown, the magnetic field decreases sharply as the distance increases from the interpolar gap surface; therefore, the flow channel's minimal thickness is essential for optimal magnetization of the IM labeled CTCs. The dimensions of the individual flow channel were experimentally determined (see the supplementary material).

TABLE II. Influence of slide thickness on the maximal magnetic field magnitude at the interpolar gap edges (L and R correspond to the left and right edges of the interpolar gap, respectively).

	B (T)							
	Gap 1		Gap 2		Gap 3		Gap 4	
Slide Thickness (mm)	L	R	L	R	L	R	L	R
0.08	1.71	1.69	1.64	1.64	1.64	1.64	1.69	1.71
0.11	1.61	1.59	1.53	1.53	1.53	1.53	1.59	1.61
0.13	1.55	1.53	1.48	1.48	1.48	1.48	1.53	1.55
0.15	1.51	1.49	1.43	1.43	1.43	1.43	1.49	1.51

The flow channel is formed by tightening permanent O-ring seals placed in a curved groove at the cassette's front side toward the coverslip slide and the magnetic core. EPDM O-ring seals with 50 Shore A hardness were selected due to their low hardness and good chemical resistance. The load required to facilitate a leakage-free flow channel of a single O-ring was experimentally found using a compression test. The compression test revealed that a load of 16.5 N is required to deform a single O-ring by 0.35 mm (at 20% deformation of the initial O-ring width). While the external applied load necessary for the tightening of a single O-ring is achievable quite easily, the formation of 100 leakage-free flow chambers (corresponding to the compression of 100 O-rings) requires the generation of 1650 N continuously.

The cassette-magnetic core tightening system was thus designed to meet the following requirements: (1) Facilitate continuous axial load (for several hours), (2) fully automated and controllable, (3) load-based control, (4) high accuracy and repeatability, (5) facilitate dispersed load over the cassette, (6) minimal maintenance, (7) minimal size and weight, (8) horizontal installation option, and (9) equal dispersion of the load over all 100 flow chambers. An electrical-based linear actuator meets the above-mentioned requirements; thus, it was selected as most suitable for tightening.

The isolation of the loads applied by the tightening system on the outer system enclosure is essential to prevent its mechanical failure. An isolation frame was designed to absorb the subjected load and eliminate the applied stress on the enclosure unit [Fig. 9(a)]. A 3D FEA structural static analysis was performed to validate that the designed frame absorbs the applied loads with minimal displacements of its structural elements [Figs. 9(b) and 9(c)]. The ANSYS structural software was used to solve the linear static structural analysis. The 3D problem was simplified and analyzed. Structural elements of the tightening assembly, which do not influence the solution, were eliminated from the FEA model [Figs. 9(a)–9(c)]. Material definition was performed, according to the material selection design. For analysis settings, boundary conditions of fixed support were defined: top and bottom surfaces of the back plate (magnetic core side) and displacement support ($u_x = u_z = 0$, u_y = free). To be on the safe side, a safety factor was added to the estimated applied load (4000 N dispersed on the corresponding surface area perpendicular to the simplified cassette). This simulates the subjected compression load on the frame. 3D geometry meshing was performed using both hexagonal and tetrahedral mesh elements, with consideration of the modeled geometry. The solution analysis was repeated until convergence of the displacements was achieved, each iteration accompanied by mesh refinement at the critical inspected areas.

The FEA simulation confirmed that all inspected frame structure elements show considerably small displacements. Furthermore, the resulting stresses were, without exception, substantially lower than the yield strength specification of the materials selected for the cassette-magnet sealing subsystem. This implies a linear elastic material behavior (i.e., without nonlinear material plasticity behavior). Hence, after tightening, the load will discharge and the frame elements will recover to their original form. This ensures a proper,

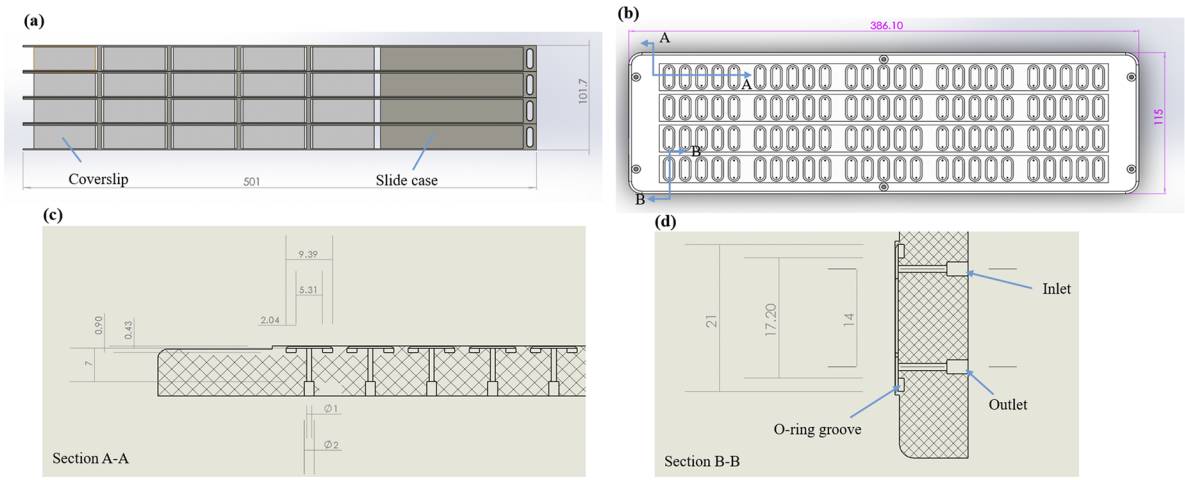

FIG. 8. (a) Top view of a coverslip slide rack allowing the installation of 20 slides. (b) Top view of the designed cassette with general dimensions. (c) Cross sectional view (A–A) from figure (b) of five O-ring grooves. (d) Cross sectional view (B–B) from figure (b) of a single O-ring groove. All dimensions are in mm.

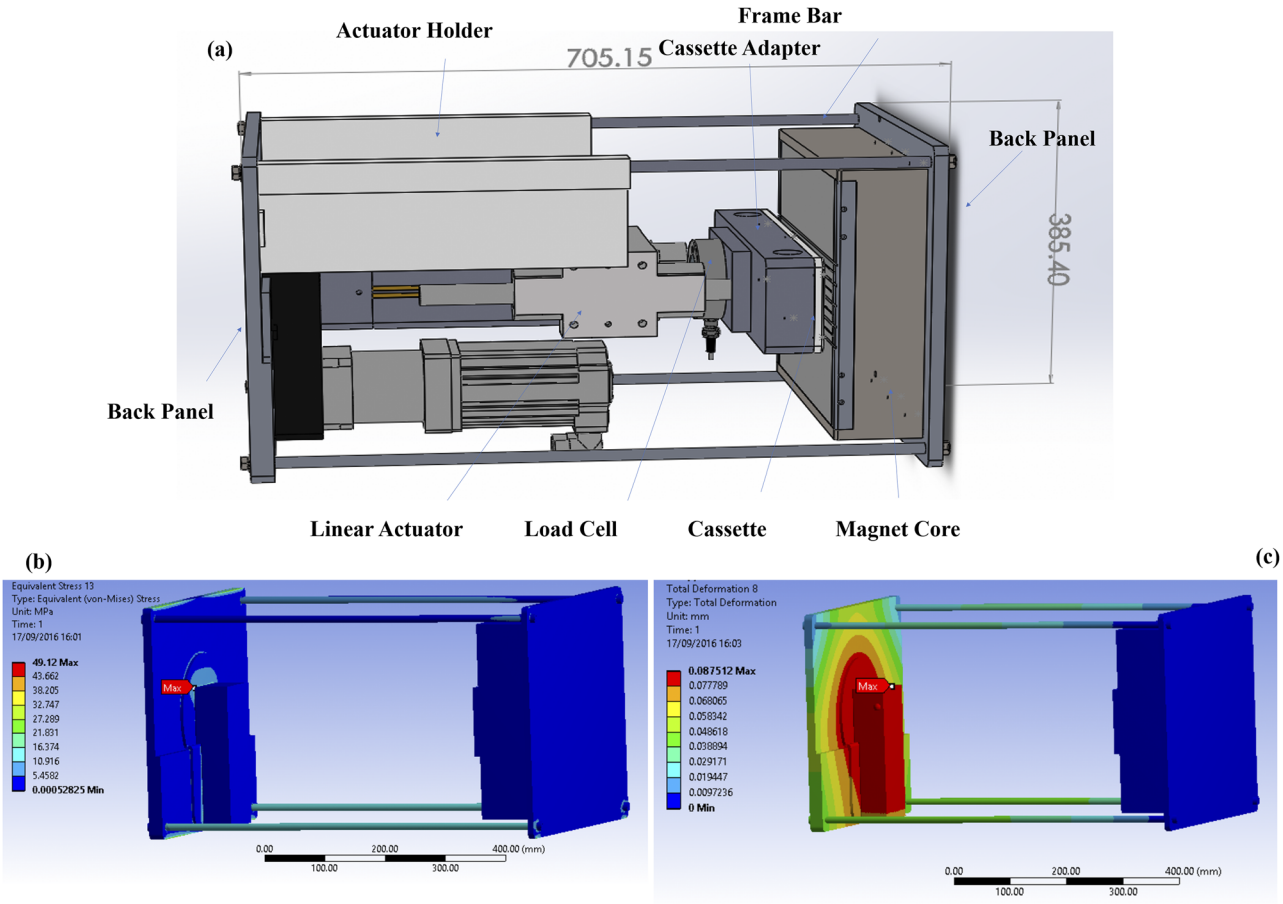

FIG. 9. (a) Tightening subsystem assembly. 3D mechanical FEA simulation results (isometric view) of a simplified tightening subsystem: (b) equivalent (von Mises) stresses and (c) total displacement.

long service life of an independent cassette-magnetic core tightening subsystem, with minimal effect on the system's enclosure unit.

VI. CONCLUSIONS

Here, a design of a high-throughput bio-ferrography-based CTC isolation medical device is presented. The system design is based on an optimized procedure for bio-ferrographic isolation of CTCs from HWB and takes into account the needs of different interested parties, e.g., the operator, medical doctor, and hospital. The designed system allows the effective IMI in 100 flow channels, suitable for 20 patients simultaneously. For each patient, only 1 ml blood sample per channel is required. The design of two main subsystems is described herein—controlled flow subsystem and magnetic-based isolation subsystem. The new flow system allows the efficient delivery of the reagents in a controlled and accurate manner for the IM labeling of CTCs in the blood samples. The designed flow system also promotes automatic priming, isolation, and system recovery procedures. On top of that, the design of a new high-gradient magnetic core with four extended interpolar gaps in a parallel configuration that allows running 20 slides simultaneously with the most compact dimensional configuration is presented. The novel design of the magnetic core was validated using FEA magnetostatic simulation and calibrated by physical measurements on Bio-Ferrograph 2100. The results confirmed that the maximal absolute magnetic field magnitude is at the interpolar edges, where the magnitude of the magnetic field decreases sharply as the distance increases from the surface of the interpolar gaps. Interestingly, the maximal magnetic field magnitude exhibits a "bath" type distribution between the four parallel interpolar gaps, where the magnetic field at the interior gaps is slightly lower (by ~0.08 T) than at external gaps. The magnetic field magnitude at all four interpolar gaps was analyzed according to the used coverslip slide's tolerance thickness integrated into the system. The results show that the CTCs that pass through the magnetic core are subjected to a magnetic field in the range of 1.43–1.71 T, depending on the coverslip slide thickness and the gap location. The presented magnetic core design was confirmed to produce a suitable magnetic field for an efficient magnetization of CTCs. Following the CTC isolation process, the isolated cells can be further counted and identified using advanced artificial neural network-aided driven microscopy techniques and characterized by complementary chemical, biological, and mechanical analyses. Overall, the presented high-throughput bio-ferrography-based CTC isolation medical device may serve as an important decision-making tool for medical doctors when monitoring cancer patients in a hospital setting. It opens a new route for early diagnosis, prognosis, and treatment of cancers, as well as other diseases, for example, osteoarthritis.

SUPPLEMENTARY MATERIAL

See the supplementary material for the determination of the flow channel dimensions and topological system operation.

ACKNOWLEDGMENTS

The authors wish to express their sincere gratitude to Professor Itai Benhar for brain storming and Mr. Mario Levenshtein for technical assistance.

REFERENCES

[1]N. Eliaz, "Wear particle analysis," in *ASM Handbook*, Friction, Lubrication, and Wear Technology Vol. 18, edited by G. E. Totten (ASM International, Materials Park, OH, 2017), pp. 1010–1031.
[2]N. Eliaz and K. Hakshur, "Fundamentals of tribology and the use of ferrography and bio-ferrography for monitoring the degradation of natural and artificial joints," in *Degradation of Implant Materials*, edited by N. Eliaz (Springer, NY, 2012), pp. 253–302.
[3]W. W. Seifert and V. C. Westcott, "A method for the study of wear particles in lubricating oil," Wear **21**, 27–42 (1972).
[4]O. Levi and N. Eliaz, "Failure analysis and condition monitoring of an open-loop oil system using ferrography," Tribol. Lett. **36**, 17–29 (2009).
[5]W. W. Seifert, V. C. Westcott, and J. B. Desjardins, "Flow unit for ferrographic analysis," US patent 5714059 (3 February 1998).
[6]J. B. Desjardins, W. W. Seifert, R. S. Wenstrup, and V. C. Westcott, "Ferrographic apparatus," US patent 6303030 (16 October 2001).
[7]O. Levi, A. Shapira, B. Tal, I. Benhar, and N. Eliaz, "Isolating epidermal growth factor receptor overexpressing carcinoma cells from human whole blood by bio-ferrography," Cytometry, Part B **88**, 136–144 (2015).
[8]N. Parkansky, B. Alterkop, R. L. Boxman, G. Leitus, O. Berkh, Z. Barkay, Y. Rosenberg, and N. Eliaz, "Magnetic properties of carbon nano-particles produced by a pulsed arc submerged in ethanol," Carbon **46**, 215–219 (2008).
[9]M. Zborowski, C. B. Fuh, R. Green, N. J. Baldwin, S. Reddy, T. Douglas, S. Mann, and J. J. Chalmers, "Immunomagnetic isolation of magnetoferritin-labeled cells in a modified ferrograph," Cytometry **24**, 251–259 (1996).
[10]P. Zhang, W. P. Johnson, and R. Rowland, "Bacterial tracking using ferrographic separation," Environ. Sci. Technol. **33**, 2456–2460 (1999).
[11]P. Zhang and W. P. Johnson, "Rapid selective ferrographic enumeration of bacteria," J. Magn. Magn. Mater. **194**, 267–274 (1999).
[12]P. Johnson, P. Zhang, M. E. Fuller, T. D. Scheibe, B. J. Mailloux, T. C. Onstott, M. F. Deflaun, S. S. Hubbard, J. Radtke, W. P. Kovacik, and W. Holben, "Ferrographic tracking of bacterial transport in the field at the narrow channel focus area, Oyster, VA," Environ. Sci. Technol. **35**, 182–191 (2001).
[13]W. P. Johnson, P. Zhang, P. M. Gardner, M. E. Fuller, and M. F. DeFlaun, "Evidence for detachment of indigenous bacteria from aquifer sediment in response to arrival of injected bacteria," Appl. Environ. Microbiol. **67**, 4908–4913 (2001).
[14]M. E. Fuller, B. J. Mailloux, P. Zhang, S. H. Streger, J. A. Hall, S. N. Vainberg, A. J. Beavis, W. P. Johnson, T. C. Onstott, and M. F. DeFlaun, "Field-scale evaluation of CFDA/SE staining coupled with multiple detection methods for assessing the transport of bacteria in situ," FEMS Microbiol. Ecol. **37**, 55–66 (2001).
[15]M. F. DeFlaun, M. E. Fuller, P. Zhang, W. P. Johnson, B. J. Mailloux, W. E. Holben, W. P. Kovacik, D. L. Balkwill, and T. C. Onstott, "Comparison of methods for monitoring bacterial transport in the subsurface," J. Microbiol. Methods **47**, 219–231 (2001).
[16]P. Zhang, W. P. Johnson, T. D. Scheibe, K.-H. Choi, F. C. Dobbs, and B. J. Mailloux, "Extended tailing of bacteria following breakthrough at the narrow channel focus area, Oyster, Virginia," Water Resour. Res. **37**, 2687–2698, https://doi.org/10.1029/2000wr000151 (2001).
[17]W. P. Johnson and W. O. McIntosh, "Tracking of injected and resident (previously injected) bacterial cells in groundwater using ferrographic capture," Microbiol. Methods **54**, 153–164 (2003).
[18]L. A. Drake, A. E. Meyer, R. L. Forsberg, R. E. Baier, M. A. Doblin, S. Heinemann, W. P. Johnson, M. Koch, P. A. Rublee, and F. C. Dobbs, "Potential invasion of microorganisms and pathogens via 'interior hull fouling': Biofilms inside ballast water tanks," Biol. Invasions **7**, 969–982 (2005).
[19]Y. Tada, T. Dohi, T. Horiuchi, P. S. Malchesky, and M. Zborowski, "Study on analytical magnetic separation system of bacterial species," J. Life Support Technol. **4**, 17 (1991).
[20]M. Zborowski, P. S. Malchesky, S. R. Savon, R. Green, G. S. Hall, and Y. Nosé, "Modification of ferrography method for analysis of lymphocytes and bacteria," Wear **142**, 135–149 (1991).

[21] M. Zborowski, P. S. Malchesky, T.-F. Jan, and G. S. Hall, "Quantitative separation of bacteria in saline solution using lanthanide Er(III) and a magnetic field," J. Gen. Microbiol. **138**, 63–68 (1992).
[22] M. Zborowski, Y. Tada, P. S. Malchesky, and G. S. Hall, "Dark-field microscopy analysis of the magnetic deposition of bacteria on a glass surface," Colloids Surf., A **77**, 209–218 (1993).
[23] L. R. Moore, M. Zborowski, L. Sun, and J. J. Chalmers, "Lymphocyte fractionation using immunomagnetic colloid and a dipole magnet flow cell sorter," J. Biochem. Biophys. Methods **37**, 11–33 (1998).
[24] K. Melnik, J. Sun, A. Fleischman, S. Roy, M. Zborowski, and J. J. Chalmers, "Quantification of magnetic susceptibility in several strains of Bacillus spores: Implications for separation and detection," Biotechnol. Bioeng. **98**, 186–192 (2007).
[25] D. Sumari, B. T. Grimberg, D. A. Blankenship, J. Mugasa, K. Mugittu, L. Moore, P. Gwakisa, and M. Zborowski, "Application of magnetic cytosmear for the estimation of *Plasmodium falciparum* gametocyte density and detection of asexual stages in asymptomatic children," Malar. J. **15**, 113 (2016).
[26] P. A. Zimmerman, J. M. Thomson, H. Fujioka, W. E. Collins, and M. Zborowski, "Diagnosis of malaria by magnetic deposition microscopy," Am. J. Trop. Med. Hyg. **74**, 568–572 (2006).
[27] S. Karl, M. David, L. Moore, B. T. Grimberg, P. Michon, I. Mueller, M. Zborowski, and P. A. Zimmerman, "Enhanced detection of gametocytes by magnetic deposition microscopy predicts higher potential for *Plasmodium falciparum* transmission," Malar. J. **7**, 66 (2008).
[28] J. S. Ishay, Z. Barkay, N. Eliaz, M. Plotkin, S. Volynchik, and D. J. Bergman, "Gravity orientation in social wasp comb cells (Vespinae) and the possible role of embedded minerals," Naturwissenschaften **95**, 333–342 (2008).
[29] K. Mendel, N. Eliaz, I. Benhar, D. Hendel, and N. Halperin, "Magnetic isolation of particles suspended in synovial fluid for diagnostics of natural joint chondropathies," Acta Biomater. **6**, 4430–4438 (2010).
[30] K. Hakshur, I. Benhar, Y. Bar-Ziv, N. Halperin, D. Segal, and N. Eliaz, "The effect of hyaluronan injections into human knees on the number of bone and cartilage wear particles captured by bio-ferrography," Acta Biomater. **7**, 848–857 (2011).
[31] D. M. Meyer, A. Tillinghast, N. C. Hanumara, and A. Franco, "Bio-ferrography to capture and separate polyethylene wear debris from hip simulator fluid and compared with conventional filter method," J. Tribol. **128**, 436–441 (2006).
[32] J. J. Elsner, Y. Mezape, K. Hakshur, M. Shemesh, E. Linder-Ganz, A. Shterling, and N. Eliaz, "Wear rate evaluation of a novel polycarbonate-urethane cushion form bearing for artificial hip joints," Acta Biomater. **6**, 4698–4707 (2010).
[33] J. J. Elsner, M. Shemesh, Y. Mezape, M. Levenshtein, K. Hakshur, A. Shterling, E. Linder-Ganz, and N. Eliaz, "Long-term evaluation of a compliant cushion form acetabular bearing for hip joint replacement: A 20 million cycles wear simulation," J. Orthop. Res. **29**, 1859–1866 (2011).
[34] B. Fang, M. Zborowski, and L. R. Moore, "Detection of rare MCF-7 breast carcinoma cells from mixture of human peripheral leukocytes by magnetic deposition analysis," Cytometry **36**, 294–302 (1999).
[35] P. B. Turpen, "Isolation of cells using bioferrography," Cytometry **42**, 324 (2000).
[36] O. Levi, B. Tal, S. Hileli, A. Shapira, I. Benhar, P. Grabov, and N. Eliaz, "Optimization of EGFR high positive cell isolation procedure by design of experiments methodology," Cytometry, Part B **88**, 338–347 (2015).
[37] D. Svetlizky, O. Levi, I. Benhar, and N. Eliaz, "Mechanical properties of bio-ferrography isolated cancerous cells studied by atomic force microscopy," J. Mech. Behav. Biomed. Mater. **91**, 345–354 (2019).
[38] M. Zborowski and J. J. Chalmers, "Rare cell separation and analysis by magnetic sorting," Anal. Chem. **83**, 8050–8056 (2011).
[39] P. S. Williams, L. R. Moore, P. Joshi, M. Goodin, M. Zborowski, and A. Fleischman, "Microfluidic chip for graduated magnetic separation of circulating tumor cells by their epithelial cell adhesion molecule expression and magnetic nanoparticle binding," J. Chromatogr. A **1637**, 461823 (2021).
[40] H. Pei, L. Li, Z. Han, Y. Wang, and B. Tang, "Recent advances in microfluidic technologies for circulating tumor cells: Enrichment, single-cell analysis, and liquid biopsy for clinical applications," Lab Chip **20**, 3854–3875 (2020).
[41] F. S. Iliescu, D. P. Poenar, F. Yu, M. Ni, K. H. Chan, I. Cima, H. K. Taylor, I. Cima, and C. Iliescu, "Recent advances in microfluidic methods in cancer liquid biopsy," Biomicrofluidics **13**, 041503 (2019).
[42] X. Li, Y. Li, W. Shao, Z. Li, R. Zhao, and Z. Ye, "Strategies for enrichment of circulating tumor cells," Transl. Cancer Res. **9**, 2012–2025 (2020).
[43] V. Akpe, T. H. Kim, C. L. Brown, and I. E. Cock, "Circulating tumour cells: A broad perspective," J. R. Soc., Interface **17**, 20200065 (2020).
[44] P. Bankó, S. Y. Lee, V. Nagygyörgy, M. Zrínyi, C. H. Chae, D. H. Cho, and A. Telekes, "Technologies for circulating tumor cell separation from whole blood," J. Hematol. Oncol. **12**, 48 (2019).
[45] A. Xiang, M. Xue, F. Ren, L. Wang, Z. Ye, D. Li, Q. Ji, G. Ji, and Z. Lu, "High-throughput and continuous flow isolation of rare circulating tumor cells and clusters in gastric cancer from human whole blood samples using electromagnetic vibration-based filtration," Oncol. Rep. **43**, 1975–1985 (2020).
[46] M. Vacante, R. Ciuni, F. Basile, and A. Biondi, "The liquid biopsy in the management of colorectal cancer: An overview," Biomedicines **8**, 308 (2020).
[47] C. R. C. Tan, L. Zhou, and W. S. El-Deiry, "Circulating tumor cells versus circulating tumor DNA in colorectal cancer: Pros and cons," Curr. Colorectal Cancer Rep. **12**, 151–161 (2016).
[48] K. C. Andree, G. van Dalum, and L. W. M. M. Terstappen, "Challenges in circulating tumor cell detection by the CellSearch system," Mol. Oncol. **10**, 395–407 (2016).
[49] Z. Habli, W. AlChamaa, R. Saab, H. Kadara, and M. L. Khraiche, "Circulating tumor cell detection technologies and clinical utility: Challenges and opportunities," Cancers **12**, 1930 (2020).
[50] J. Kraan, M. H. Strijbos, A. M. Sieuwerts, J. A. Foekens, M. A. den Bakker, C. Verhoef, S. Sleijfer, and J. W. Gratama, "A new approach for rapid and reliable enumeration of circulating endothelial cells in patients," J. Thromb. Haemostasis **10**, 931–939 (2012).
[51] W. J. Allard, J. Matera, M. C. Miller, M. Repollet, M. C. Connelly, C. Rao, A. G. J. Tibbe, J. W. Uhr, and L. W. M. M. Terstappen, "Tumor cells circulate in the peripheral blood of all major carcinomas but not in healthy subjects or patients with nonmalignant diseases," Clin. Cancer Res. **10**, 6897–6904 (2004).
[52] N. Eliaz, O. Levi, D. Svetlizky, and I. Benhar, "A high-throughput semi-automated magnetic isolation and concentration system," US provisional patent application 63/170,451 (3 April 2021).
[53] H. Birkhofer, J. Jänsch, and H. Kloberdanz, "An extensive and detailed view of the application of design methods and methodology in industry," in *Proceedings of the International Conference on Engineering Design (ICED05)* (The Design Society, Melbourne, Australia, 2005), pp. 276–277.
[54] P. Monk, *Finite Element Methods for Maxwell's Equations* (Oxford University Press, UK, 2003).
[55] D. Svetlizky, "Bio-ferrography: Mechanical properties of isolated cancerous cells by atomic force microscope and design of a multichannel ferrograph for isolation of cancerous cells from whole blood," M.Sc. thesis, Tel Aviv University, Israel, 2017.
[56] O. Levi, "Diagnosis of colorectal cancer by bio-ferrography," Ph.D. dissertation (Tel Aviv University, Tel Aviv, Israel 2015).
[57] P. Nath, J. Strelnik, A. Vasanji, L. R. Moore, P. S. Williams, M. Zborowski, S. Roy, and A. J. Fleischman, "Development of multistage magnetic deposition microscopy," Anal. Chem. **81**, 43–49 (2009).
[58] J. Sun, L. Moore, W. Xue, J. Kim, M. Zborowski, and J. J. Chalmers, "Correlation of simulation/finite element analysis to the separation of intrinsically magnetic spores and red blood cells using a microfluidic magnetic deposition system," Biotechnol. Bioeng. **115**, 1288–1300 (2018).